Flow, Turbulence and Combustion **72:** 463–492, 2004.
© 2004 *Kluwer Academic Publishers. Printed in the Netherlands.*

Effect of Roughness on Wall-Bounded Turbulence

KIRAN BHAGANAGAR[1], JOHN KIM[1] and GARY COLEMAN[2]
[1]*Department of Mechanical and Aerospace Engineering, University of California, Los Angeles, Los Angeles, CA, U.S.A., E-mail: jkim@seas.ucla.edu*
[2]*School of Engineering Sciences, University of Southampton, Southampton, U.K.*

Received 3 October 2003; accepted in revised form 11 January 2004

Abstract. Direct numerical simulation of turbulent incompressible plane-channel flow between a smooth wall and one covered with regular three-dimensional roughness elements is performed. While the impact of roughness on the mean-velocity profile of turbulent wall layers is well understood, at least qualitatively, the manner in which other features are affected, especially in the outer layer, has been more controversial. We compare results from the smooth- and rough-wall sides of the channel for three different roughness heights of $h^+ = 5.4$, 10.8, and 21.6 for Re_τ of 400, to isolate the effects of the roughness on turbulent statistics and the instantaneous turbulence structure at large and small scales. We focus on the interaction between the near-wall and outer-layer regions, in particular the extent to which the near-wall behavior influences the flow further away from the surface. Roughness tends to increase the intensity of the velocity and vorticity fluctuations in the inner layer. In the outer layer, although the roughness alters the velocity fluctuations, the vorticity fluctuations are relatively unaffected. The higher-order moments and the energy budgets demonstrate significant differences between the smooth-wall and rough-wall sides in the processes associated with the wall-normal fluxes of the Reynolds shear stresses and turbulence kinetic energy. The length scales and flow dynamics in the roughness sublayer, the spatially inhomogeneous layer within which the flow is directly influenced by the individual roughness elements, are also examined. Alternative mechanisms involved in producing and maintaining near-wall turbulence in rough-wall boundary layers are also considered. We find that the strength of the inner/outer-layer interactions are greatly affected by the size of the roughness elements.

1. Introduction

Surface roughness is a defining feature of many of the high Reynolds-numbers flows found in engineering. In fact, the higher the Reynolds number, the more likely the effects of roughness are significant, since the size of the roughness elements becomes increasingly large compared to the near-surface viscous length appropriate for smooth-wall flows. As a result, turbulent boundary layers over the hulls of ships and submarines, within turbo-machinery, and over the surface of the earth are all cases to which the smooth-wall idealization rarely applies. Unfortunately, the impact of surface roughness is not entirely understood, and a number of important fundamental questions have not yet received a satisfactory answer.

The turbulent boundary layer over a rough surface contains a roughness sublayer, within which the flow is directly influenced by the individual roughness elements

and is therefore not spatially homogeneous (i.e. time-averaged statistics are not independent of location, at the same mean wall-normal distance). The height of this sublayer presumably depends upon the height of the roughness elements, as well as their shape and density distribution. Plane averaging over a repeating unit of a uniform array will lead to a representative profile within the roughness sublayer, which could then be regarded as spatially homogeneous on scales larger than the unit, if it is much larger than the lateral size of individual elements. This type of unit averaging has been done by Raupach et al. [1], Wood and Mason [2], and Cheng and Castro [3]. The questions that arise, which we attempt to answer below for one type of representative roughness, are (1) What is the height of the roughness sublayer and how does it compare to the other length scales of the roughness? (2) What is the significance of the roughness sublayer with respect to the dynamics of turbulence in this region? (3) Are the turbulent statistics in the logarithmic region independent of the flow in the roughness sublayer? and if not, (4) How do the turbulence structures generated within the sublayer interact with and determine the eddy structure in the log region?

Perry et al. [4] performed experiments using both three-dimensional (3D) diamond-shaped mesh roughness with height 29 mm (0.3δ, where δ is the boundary layer thickness for the smooth-wall turbulent boundary layer) and streamwise and spanwise mesh dimensions respectively of 10.5 mm (0.1δ) and 1.5 mm (0.01δ). They also considered a two-dimensional (2D) wavy surface with peak-to-valley normalized height of 17 mm (0.1δ) and streamwise wavelength of 76 mm (0.8δ). In both cases they observed that smooth- and rough-wall boundary layers have quite different structures and are controlled by different length scales in the inner layer, but that low-order statistics are similar well away from the surface, implying that the outer layer is unaffected by the details of the surface, be it smooth or rough. Raupach et al. [1] present other data, laboratory and atmospheric, that reinforce the outer-layer similarity hypothesis. However, there is other evidence, as described below, that in some cases the turbulence over rough surfaces can be very different from that over smooth surfaces throughout the boundary layer.

The experiments of Krogstad et al. [5] used a rough surface consisting of a square mesh of wire diameter 0.69 mm (0.01δ), wire centerline spacing 3.18 mm (0.04δ) and screen thickness of 1.55 mm (0.02δ). Antonia and Krogstad [6] used 2D rods in spanwise direction with diameter 1.6 mm (0.02δ) and height 1.6 mm (0.02δ). Tachie et al. [7] used three different surface roughness: the first one a perforated plate with holes of diameter 2.2 mm (0.04δ) and thickness of 1.4 mm (0.03δ); the next one sand grain roughness of 1.2 mm (0.02δ); and the third a square mesh of wire diameter 0.6 mm (0.01δ) with wire centerline spacing of 7 mm (0.15δ). Keirsbulk et al. [8] used roughness elements consisting of 2D square bars with dimension of 3 mm (0.05δ) with the axes of the bars placed along the flow direction. George and Simpson [9] performed experiments for 2D turbulent boundary layers with sparsely and uniformly distributed 3D roughness elements; the roughness elements were circular cylinder roughness elements with diameter 0.6 mm (0.01δ),

spacing in streamwise- and spanwise- directions 1.8 mm (0.03δ), and for three different roughness heights 0.3 mm (0.0075δ), 0.6 mm (0.01δ) and 1.2 mm (0.02δ). More recently, 2D roughness has been investigated by Ashrfian and Andersson [10] using direct numerical simulations (DNS) at Reynolds number based on the mean pressure-gradient of 400. Two-dimensional square rods, periodically arranged in the streamwise direction, with a roughness height of 0.034δ, where δ is the half-channel width, were introduced on both walls of the channel. They observed the values of all components of the Reynolds stress tensor were modified in the inner-layer as well as outer-layers due to the presence of roughness. Leonardi et al. [11] investigated the effect of square bars on the bottom wall in a turbulent channel flow using DNS for four different values of longitudinal separation (w) to the height (k) ratios of (1, 3, 7, 19). They observed increased coherence in the spanwise direction and decreased coherence in the streamwise direction with increasing w/k ratio.

All these experiments demonstrate significant differences in the shear stress, $\overline{uv}$, and root-mean-square (rms) of fluctuating velocity components *throughout* the inner- and outer-layer. Shafi and Antonia [12] measured the rms vorticity fluctuations normalized by the friction velocity u_τ and boundary-layer thickness δ, and found a moderate increase of the wall-normal and spanwise components in the outer layer. They concluded that the effect of roughness on the vorticity is less pronounced than on the Reynolds stresses. These results conflict with the traditional picture of wall similarity, which assumes that outside the roughness sublayer the turbulent motions are independent of the details of the (smooth or rough) surface at sufficiently large Reynolds numbers.

To get a clearer picture of the impact of roughness in turbulent wall layers, we investigate the effects of 3D roughness arranged in an "egg-carton" shape (see Section 2) on turbulent boundary layers, and differences between the rough- and smooth-wall flows. It is important to identify the physical mechanisms responsible for the production and maintenance of turbulence adjacent to a rough wall, and to ascertain if they are similar to those in the smooth-wall boundary layer, or if instead alternative mechanisms are involved (this has profound implications, for example, for control strategies applied to rough-wall flows). We investigate the physical mechanisms represented by the various terms in the transport equations for the Reynolds stresses, and consider whether alternatives (such as wakes induced by the roughness elements [13]) are involved in the turbulence production process in the inner region.

In light of the full range of experimental results, it now appears that rough-wall boundary layers can be categorized according to whether or not the surface roughness affects the outer layer (although to some extent this classification will depend on which statistic is examined). Some of the above researchers have hypothesized that the exact nature of the roughness surface is the differentiating parameter—i.e. that some surfaces "communicate" with the outer layer while others do not, despite the fact that they may produce similar first-order statistics (and thereby

equivalent sand-grain roughness) or even share some geometric features (such as mean height or spacing). Hence, there is a need to fully understand the influence of roughness geometry. To do this, it is necessary to identify the relevant parameters and study their influence on the turbulence dynamics. Possible parameters include the size and shape of the roughness elements (and whether or not there is a heterogeneous range of each, or simply a repeating pattern of a single "unit cell"), and their streamwise and spanwise distribution (spacing, alignment and density). A number of studies of the effect of roughness height of various element shapes have already been done. One of the aims of this paper is to categorize the influence of roughness for a single generic 3D element shape of fixed height, in terms of the other geometric parameters (streamwise and spanwise spacing), and to quantify how these parameters do or do not affect the outer layer. So far, little has been attempted in this direction. The results are expected to provide a useful guide as to when outer-layer similarity holds, and for what statistics, for rough-wall boundary layers.

The paper is organized as follows. Section 2 deals with the numerical approach. In Section 3 we discuss the effect of 3D roughness on the large-scale and small-scale features of the roughness-sublayer (RSL), the inner (containing the RSL) and outer layers, for one class of turbulent rough-wall boundary layer. Next we discuss the physical mechanisms involved in the production and maintenance of turbulence adjacent to and well away from the rough-wall side of the channel. (It should be noted that for small roughness heights, as in the present case, the roughness sublayer is part of the inner layer. In cases such as meteorological flows with large roughness heights (e.g. buildings), the roughness sublayer can extend into the outer layer, and the analysis will be more complicated than that presented here.) In Section 4 we show the results for various numerical experiments conducted with different roughness surfaces. This is followed by a summary in Section 5.

In this paper, u, v, w denote the velocity fluctuations in the streamwise (x), wall-normal (y) and spanwise (z) directions, respectively. The superscript $^+$ denotes a quantity normalized by the wall-shear velocity, u_τ, and the kinematic viscosity, ν.

2. Numerical Approach

We have developed a numerical tool to simulate turbulent flow over a complex boundary while retaining the simplicity and efficiency of computation in a Cartesian system. This was done using an immersed boundary method (IBM) [14]. The concept and details of this approach can be found in [15–17]. The equations of fluid motion are calculated on the regular geometry of a periodic channel. The virtual roughness boundary σ is prescribed within the channel as a function of the streamwise (x) and spanwise (z) variables, such that the active flow domain D is given by $D = (x, y, z)|y = \sigma(x, z)$. To enforce the no-slip condition at this virtual boundary, a linear profile is assumed for the streamwise and spanwise components of velocity between zero at $y = \sigma(x, z)$ and the velocity at a grid point above the

virtual boundary. The wall-normal component of velocity is prescribed from u and w, mass conservation and the no-slip condition. The immersed no-slip boundary is prescribed via a body force term. For purposes of defining the body force, we employ a first-order temporal discretization of the Navier-Stokes equations:

$$\frac{\mathbf{u}^{n+1} - \mathbf{u}^n}{\Delta t} + \mathbf{u}^n \cdot \nabla \mathbf{u}^n = -\nabla p^n + \nu \nabla^2 \mathbf{u}^n + \mathbf{f}^n, \tag{1}$$

where $\mathbf{f}^n = (f_x, f_y, f_z)^n$ is the body force, $\mathbf{u} = (u, v, w)$ the velocity vector, p the pressure, ν the kinematic viscosity, Δt the time-step increment, and the superscripts n and $n + 1$ respectively indicate the current and next time level. On the immersed boundary $\sigma(x, z)$, the velocity is zero, such that

$$\mathbf{u}^{n+1} = (0, 0, 0) \tag{2}$$

and we approximate the body force as:

$$\mathbf{f}^n = \frac{\mathbf{V} - \mathbf{u}^n}{\Delta t} + \mathbf{u}^n \cdot \nabla \mathbf{u}^n + \nabla p^n - \nu \nabla^2 \mathbf{u}^n, \tag{3}$$

where $\mathbf{V} = (0, 0, 0)$. The time-dependent body force is applied at a set of two points, the one just below the immersed boundary and the one just above. (When the boundary coincides with the grid, the body force is applied at the boundary and at a point below.) This method gives flexibility in choosing the immersed boundary not found in some other methods, since there is no need to line up the boundary with a grid. We use this method here to simulate turbulent channel flow between a smooth wall and one covered with regular 3D roughness elements. Apart from the additional forcing term, and the wall-normal discretization, the numerical method is similar to the one presented by Kim et al. [18]. We use Fourier series in the streamwise and spanwise directions. In the wall-normal direction, however, we employ a fourth-order compact finite-difference scheme instead of the Chebyshev polynomials used by Kim et al. [18]. The code has been parallelized using message-passing-interface (MPI). The parallelization strategy is based on the domain decomposition technique, since the IBM approach requires communication between the processors, which contain the interpolating velocity grid points, and those with the grid points where the body force needs to be applied. This required development of an efficient bookkeeping strategy and MPI broadcasting technique.

DNS have been performed for $Re_\tau = 400$ (Reynolds number based on wall-shear velocity u_τ and channel half-height δ) in a periodic channel of streamwise and spanwise size $L_x/\delta = 2\pi$ and $L_z/\delta = \pi$, where 2δ is the distance between the plane walls (one of which now lies outside the active flow domain, below the virtual rough surface). The spatial discretization used 256 streamwise Fourier modes, 257 wall-normal compact finite-difference grid points of fourth-order accuracy and 256 spanwise Fourier modes. In the wall-normal direction, nonuniform mesh was used. The grid spacing varied from 0.94 wall units (based on u_τ at the rough wall) adjacent to the virtual no-slip surface to 6.5 at the centerline. In the horizontal directions Δx^+ was approximately 15 and Δz^+ was approximately 8.

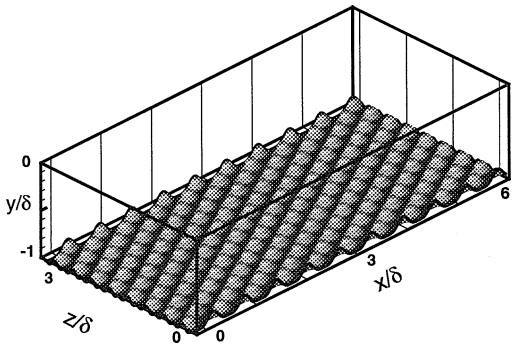

Figure 1. The roughness surface used in the simulations for $h^+ = 21.6$. The channel is shown from the lower-wall ($y = -1$) to the center of the channel ($y = 0$). The virtual no-slip roughness surface is at $\sigma = -0.96$.

The virtual no-slip surface consists of smooth 3D "egg carton"-shaped surface $\sigma(x, z)$ such that

$$\sigma(x,z) = \sigma_0 + \frac{h}{4}\left[-1 + \left(1 + \sin\left(\frac{2\pi x}{l_x} + \frac{2\pi z}{l_z}\right)\right) \times \left(1 + \sin\left(\frac{2\pi x}{l_x} - \frac{2\pi z}{l_z}\right)\right)\right], \tag{4}$$

where $\sigma(x, z)$ is measured with respect to the channel coordinates, in units of δ, h is the (peak to valley) roughness height, σ_0 defines the mean offset of the immersed boundary, and l_x and l_z are the streamwise and spanwise wavelengths (peak-to-peak distance) of the roughness elements. We chose $\sigma = -0.96$ for all simulations presented here, which prescribes the virtual no-slip roughness surface at the bottom of the DNS domain, just above the lower wall. For this surface, the roughness "bumps" extend $3h/4$ above σ_0, while the valleys lie $h/4$ below it. The roughness surface corresponding to $h^+ = 21.6$ is shown in Figure 1.

3. Turbulent Flow over a Rough-Wall with 3D Roughness Elements

3.1. Turbulence statistics

We analyze a turbulent flow over a rough-wall with 3D roughness elements using DNS. The shape of the roughness elements is expressed by Equation (4). We specify roughness elements with peak-to-peak spacing in the streamwise and spanwise directions of 100 wall units in terms of smooth-wall u_τ and three different heights of approximately $h^+ = 5.4$, 10.8 and 21.6. Unless otherwise stated, results shown here are for the case of $h^+ = 21.6$, with the other two cases included where comparison is appropriate. Once the velocity field reached a statistically steady state, the computations were continued in time for about 10 nondimensionalized units (in terms of the smooth-wall u_τ and δ) to obtain mean statistics, which were gathered

by averaging over x and z directions as well as time. Convergence was verified by examining the Reynolds shear stress, which must converge to a straight line.

The classical framework established by Nikuradse [19] predicts that the effect of roughness on the mean-velocity distribution is confined to a thin wall layer. In the log-region, assuming a logarithmic velocity distribution for flow over a smooth wall given by

$$\frac{U}{u_\tau} = \frac{1}{\kappa} \ln\left(\frac{y_w u_\tau}{\nu}\right) + C_0, \tag{5}$$

the rough-wall modification is

$$\frac{U}{u_\tau} = \frac{1}{\kappa} \ln\left(\frac{y_w u_\tau}{\nu}\right) + C_0 - \frac{\Delta U}{u_\tau}, \tag{6}$$

where $\Delta U/u_\tau = f(k_s^+)$ is the roughness function, k_s^+ the equivalent sand grain roughness, and we assume $\kappa = 0.41$; $C_0 = 5.5$ is the additive constant for both the rough- and smooth- wall, u_τ is the local wall-shear velocity (u_τ of each wall is referred to as local u_τ, hereinafter). For the smooth-wall case u_τ is obtained using the shear at the upper smooth wall, and for the rough wall u_τ is obtained from the mean momentum balance. Comparing the rough- and the smooth-wall distributions, the roughness results in a downward shift of the logarithmic profile with no discernible change in slope.

To represent the mean velocity profile over a rough surface, the first task is to determine the virtual offset α for the rough-wall side. This is done by expressing the mean velocity in the log-region in the following form

$$\frac{U}{u_\tau} = \frac{1}{\kappa} \ln\frac{(y_w - \alpha)}{y_0} \tag{7}$$

Here, α is the virtual offset, y_0 is the roughness length, and y_0 and α are determined by fitting the mean velocity profile in the inertial sublayer to the above equation. All the results shown consider the virtual offset at the rough-wall side. Figure 2 shows the mean velocity profile normalized by the local wall-shear velocity, plotted in wall units for the smooth-wall side and rough-wall side, for roughness heights of $h^+ = 5.4$, 10.8 and 21.6. In this figure, y^+ represents the distance from the wall in wall units. All results shown below compute y^+ taking the virtual offset into account and using the local u_τ unless stated otherwise. The roughness produces the expected downward shift in U^+, which increases with increasing h^+. This results also serves as a validation for our numerics. Raupach et al. [1] present a relationship between ΔU^+ and h^+ for wire screen roughness, bar roughness, sand-grain roughness and natural vegetation. For our h^+ of 21.6, the corresponding ΔU^+ is around 6.0, which is close to the value of 6.4 observed here. Ashrafian and Andersson [10] obtained ΔU^+ of 7.0 for a 2D spanwise roughness of height 0.034δ, which is higher than that given by our simulations, although not appreciably. The differences could be attributed to the difference in streamwise spacing of the roughness elements.

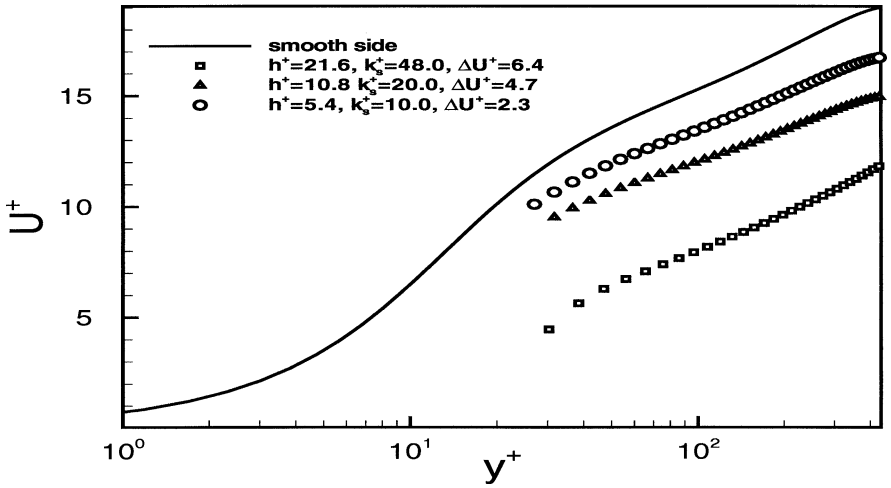

Figure 2. Mean velocity normalized by local u_τ shown for the smooth-wall side and the rough-wall side for h^+ of 5.4, 10.8, 21.6.

The three rough-wall cases correspond respectively to equivalent sand-grain roughness of $k_s^+ = 10$, 20, and 48; the ratio of k_s to the physical peak-to-valley height h for the three cases is thus 1.85, 1.85 and 2.2. These k_s/h values are analogous to Case 11 of Schlichting's regular roughness patterns [20]. This implies the "egg carton" roughness used here is comparable in terms of its effect on the mean velocity to uniformly packed spheres, with distance to diameter ratio of 0.46.

Figure 3 shows the mean-velocity defect for the smooth-wall side and the rough-wall side of the channel. Here the mean velocity is normalized by local u_τ, and the distance from the wall y_w is normalized by δ_t, where δ_t is defined as the distance from the wall to the y location corresponding to minimum rms velocity fluctuations. It is worth mentioning that the results in the outer-layer for the rough-wall and smooth-wall collapse better when scaled by δ_t compared to δ, suggesting that δ_t is a better scaling measure for the outer layer. The mean-velocity profile in the outer layer is independent of the roughness elements. This is consistent with the classical notion that roughness affects the mean velocity only in the inner layer and the mean velocity in the outer layer is unaffected by the roughness elements.

We next examine higher-order statistics. We are particularly interested in the turbulent intensities for velocity and vorticity in both the inner and outer layers, since behavior of the former allows us to infer how roughness affects the largest scales of motion, while that of the latter indicates how it alters the small-scale features.

Figure 4a shows the rms velocity fluctuations normalized by u_τ at the smooth wall. They are plotted against wall-normal distance y normalized by the channel half height δ. For the rough-wall side we present results only above the virtual origin. All three components are larger above the rough-wall than the smooth-wall,

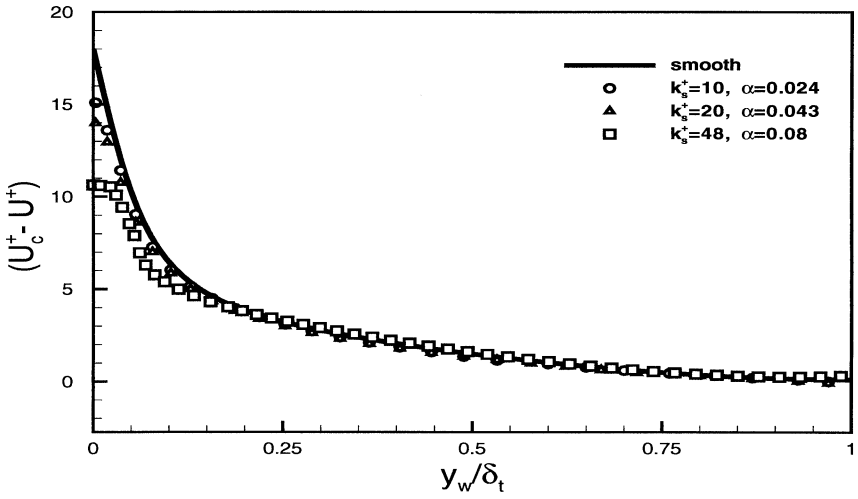

Figure 3. Mean velocity defect normalized by local u_τ. The wall-normal distance is normalized by δ_t (defined as the length from the wall to the y-location corresponding to the minimum rms velocity fluctuations from Figure 4(a)), which is the effective boundary layer thickness.

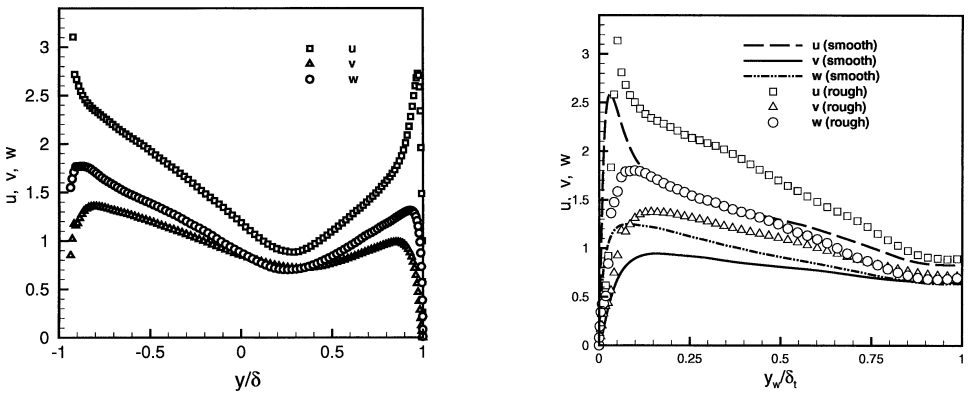

(a) (b)

Figure 4. (a) Turbulent intensity of velocity components normalized by u_τ at the smooth wall. The wall-normal distance is normalized by the channel half-height. (b) The wall-normal distance is normalized by δ_t.

showing that roughness results in an increase of turbulence intensity in agreement with existing experimental and numerical observations. The trend (not shown) is for the fluctuations to become more intense with increasing roughness height, all other parameters being the same. Moreover, the peak location moves further away from the wall, with increasing roughness. As the rough-wall layers and smooth-wall layers have different thicknesses, an appropriate scaling is required. From Figure 4a, we select δ_t corresponding to the location of the minimum velocity fluctuations from the respective wall. In Figure 4b the results with the new scaling

are shown. With this scaling all the velocity components are larger for the rough-wall compared to the smooth-wall, indicating clearly that the outer-layer is affected by roughness.

Figure 5a presents the velocity fluctuations normalized by their respective local u_τ, from the appropriate smooth or rough wall, with the distance from the wall expressed in wall units. With this normalization, the maximum streamwise fluctuation and spanwise fluctuation components near the wall are smaller for the rough-wall case than for smooth-wall, while the wall-normal component is larger for the rough-wall case. Further away from the wall, the three components are smaller for the rough-wall side. Note that although the streamwise fluctuation is larger than the smooth wall in absolute terms, it represents a smaller fraction of the local u_τ (which now includes both pressure and viscous drag). Figure 5b shows the same results now plotted in the outer units, with the distance from the wall normalized by δ_t. Away from the wall all three velocity components for the rough-wall are smaller compared to the smooth-wall. These results illustrate that for this flow the surface roughness does indeed directly affect the outer layer, and that this effect involves the large scales of motion.

Krogstad and Antonia [21] investigated two different rough surfaces, one mesh roughness and the other rod roughness, but both having a similar roughness function. For mesh roughness they observed that streamwise fluctuation decreased and the wall-normal fluctuation increased in the wall-region, similar to our results. However, for their rod roughness, both streamwise and wall-normal fluctuations decreased in the wall region. In the outer region, for both roughnesses, they observed a prominent increase for the wall-normal fluctuations as observed in our simulations. Other investigators, George and Simpson [9] among others, also reported that the streamwise fluctuations decreased while the wall-normal fluctuations increased in the inner region of rough wall.

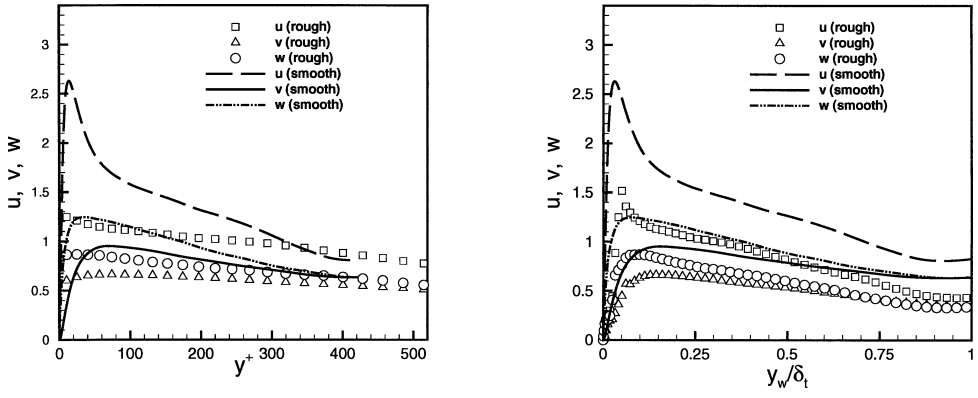

Figure 5. (a) Turbulent intensity of velocity components normalized by local u_τ and plotted in y^+. (b) The distance from the wall (y_w) is normalized by δ_t.

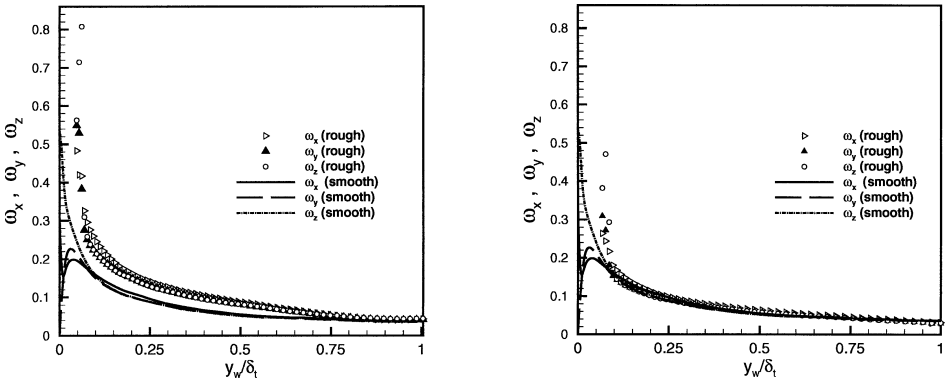

Figure 6. (a) The rms vorticity fluctuations normalized by the smooth-wall u_τ. The distance from the wall is normalized by δ_t. (b) Normalized by local u_τ.

The behavior of the small scales can be revealed by the rms vorticity fluctuations. In Figure 6a the rms vorticity fluctuations are normalized by u_τ at the smooth wall and they are plotted in terms of y_w/δ_t. Roughness results in an increase of each component of vorticity in the inner layer, in absolute terms. In Figure 6b we scale them with local u_τ. In contrast to the velocity fluctuations, the vorticity fluctuations in the outer layer are not affected by the rough wall. Further, the roughness-induced trend toward isotropy is apparent. This could be interpreted as follows: the structure of small-scale turbulence is about the same for the smooth and rough wall, in that in both cases the outer-layer vorticity is nearly isotropic and of the same magnitude. Therefore, no change in small-scale statistics is observed in the presence of roughness. The tendency toward isotropy of large-scale turbulence has been reported before. For example, Antonia and Krogstad [6] reported that rough wall resulted in an increased tendency toward isotropy from their analysis of the Reynolds stress anisotropy tensor. Using a similar approach, Leonardi et al. [11] also reported that roughness results in the tendency to isotropy.

To analyze the turbulent transport process we investigated further higher-order statistics and the turbulence energy budget. The skewness of the u velocity is defined as $S_u = \overline{u^3}/u_{\text{rms}}^3$, with similar definitions for the wall-normal v and spanwise w components, S_v and S_w, respectively. Figure 7 shows the skewness of the three velocity components S_u, S_v and S_w. The streamwise skewness changes from a positive value to a negative value for the smooth-wall side at around y^+ of 10, while for the rough-wall case the change occurs at $y^+ \approx 20$. Beyond y^+ of 30, S_v for the smooth-wall case is distinctly different compared to the rough-wall side, as S_v rough is mostly negative for the rough wall, whereas for the smooth wall it is mostly positive and changes sign at the end of the outer layer. This effect of roughness on S_v reflects a significant change in the large-scale structures in the outer region. It also suggests that the turbulence transport in the horizontal directions is not significantly affected, whereas that in the wall-normal direction is affected due

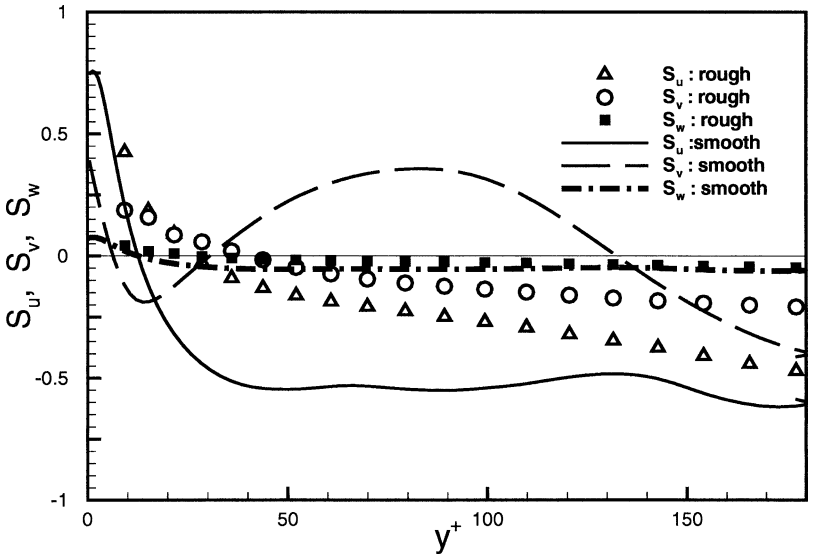

Figure 7. Skewness of velocity fluctuations: S_u, S_v and S_w respectively denote the skewness of u, v and w velocity.

to the presence of roughness. This is in agreement with an experimental observation by Cheng and Castro (Castro, private communication). Keirsbulck et al. [22] used 2D bars of square cross-section placed perpendicular to the flow direction. Their second-order statistics indicated that the outer layer was unaffected by the type of the roughness used by them. Their skewness results indicated that S_u and S_v follow the same trend for both the smooth and rough wall throughout the boundary layer, suggesting that skewness is a good indicator in determining the changes in the large scale structures in the outer layer.

The Kurtosis, or fourth-order moment, defined as $K_u = \overline{u^4}/u_{\text{rms}}^4$ is quite different near the smooth and rough-walls, but away from the wall it approaches a Gaussian value for all three components for both rough- and smooth-wall cases (not shown here). This indicates that the fourth-order statistics are affected only in the inner layer due to the presence of roughness.

The transport equation for turbulence kinetic energy $\overline{E} = \frac{1}{2}\overline{u_i u_i}$ is given by

$$\frac{\mathrm{DE}}{\mathrm{Dt}} = P + T + \Pi + D - \epsilon \,, \tag{8}$$

where

$$P = -\overline{uv}\frac{\partial U}{\partial y}, \quad T = -\frac{\partial \overline{Ev}}{\partial y}, \quad \Pi = -\frac{\partial \overline{pv}}{\partial y},$$
$$D = \frac{1}{Re_\tau}\frac{\overline{\partial^2 E}}{\partial y^2}, \quad \epsilon = \frac{1}{Re_\tau}\overline{\frac{\partial u_i}{\partial x_j}\frac{\partial u_i}{\partial x_j}} \,. \tag{9}$$

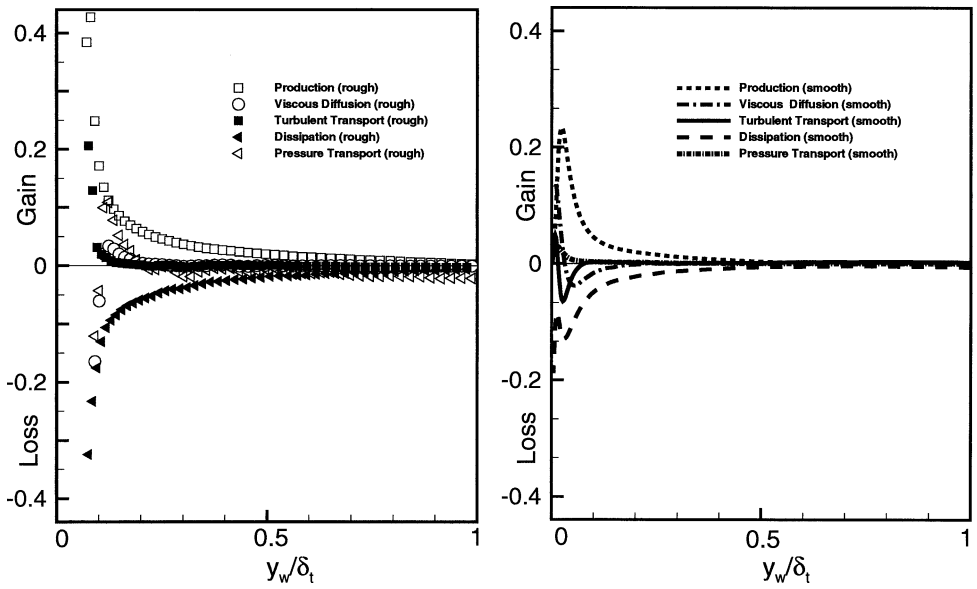

Figure 8. Terms in the turbulent kinetic energy budget normalized by u_τ at the smooth-wall.

Here, P, T, Π, D and ϵ respectively denote the rate of production, turbulent transport, pressure transport, viscous diffusion, and dissipation.

Figure 8 shows the turbulent energy budget normalized by u_τ at the smooth wall and the wall-normal distance by y_w/δ_t. Normalized in this way, the maximum production rate as well as the maximum dissipation rate at the rough-wall side is larger than those at the smooth side, as expected. The maximum value of the turbulent transport is also larger than that of the smooth-wall case. The viscous diffusion terms are different in the inner region. The pressure transport term is not of significant value and the change is limited to very close to the rough wall in spite of increased form drag due to roughness. In Figure 9, the same terms are now normalized by the local u_τ (i.e. the respective wall-shear velocity) and plotted in y^+. The production rate for the rough-wall case is less than that of the smooth-wall case. The maximum value of the turbulent transport term remains about the same. There are regions in the inner layer where the turbulent transport is toward the wall for the smooth-wall case, whereas it is always away from the wall for the rough-wall case. A similar trend is observed for the viscous diffusion term. The direction of the transport of the turbulent kinetic energy due to the turbulent velocity fluctuations as well as due to viscous stresses is different in the inner layer due to the presence of roughness; no significant difference is discernible in the outer layer. The main difference between the smooth- and rough-wall turbulent kinetic energy budget observed by Keirsbulck et al. [22] was that in the inner region, the viscous diffusion, advection and turbulent transport terms showed different trends for the rough-wall case. Krogstad and Antonia [21] reported that the major effect

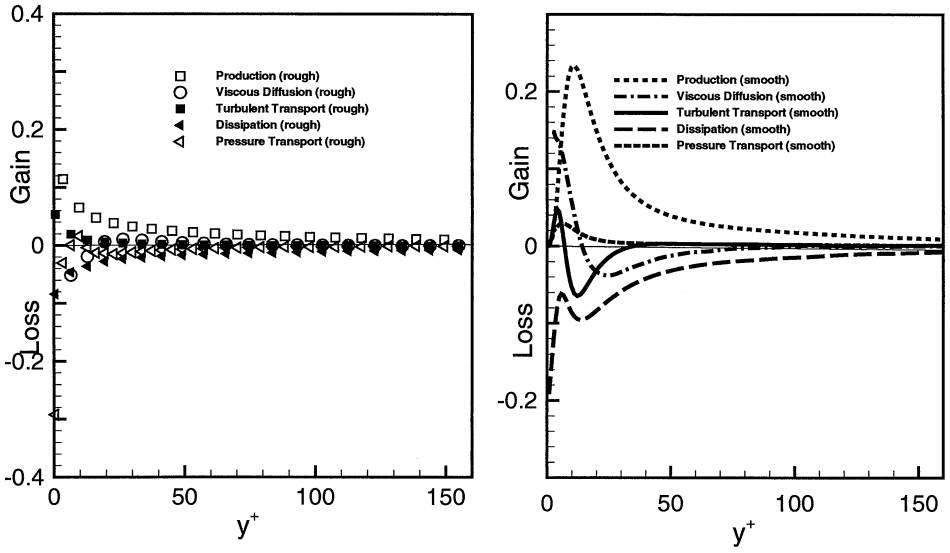

Figure 9. Terms in the turbulent kinetic energy budget normalized by local u_τ and plotted in y^+.

of roughness was in the turbulent transport term, and the direction of the turbulent transport process depended on the nature of the roughness. Our results indicate that both the turbulent transport and viscous diffusion terms are significantly modified due to roughness.

At this point, as we are interested in the turbulent transport of the turbulent structures, we concentrate on the transport term for the $\overline{u^2}$ and $\overline{uv}$ transport equation, $\overline{u^2 v}$ and $\overline{uv^2}$, respectively (the transport terms for $\overline{v^2}$, $\overline{w^2}$ are not significant compared to these terms). It is evident from Figure 10 that the transport term for $\overline{u^2}$ is significantly modified by the surface roughness, whereas that for $\overline{uv}$ is not affected significantly, indicating that the effect of surface roughness on $\overline{u^2}$ compared to other components extends much beyond the inner layer. Both the energy budget and the transport terms of the Reynolds stresses indicate a modified wall-normal transport process in the outer layer induced by the roughness. Further, the modification of the transport term due to roughness arises mainly due to the contribution from $\overline{u^2}$. This information should be valuable for turbulence modeling of rough walls.

3.2. TURBULENCE STRUCTURES

To investigate the effect of surface roughness on turbulence structures, two-point correlations of the velocity fluctuations are examined, from which the length scales associated with the near-wall streaky structures and streamwise vortices can be estimated. Figure 11 shows the two-point correlations of the streamwise and

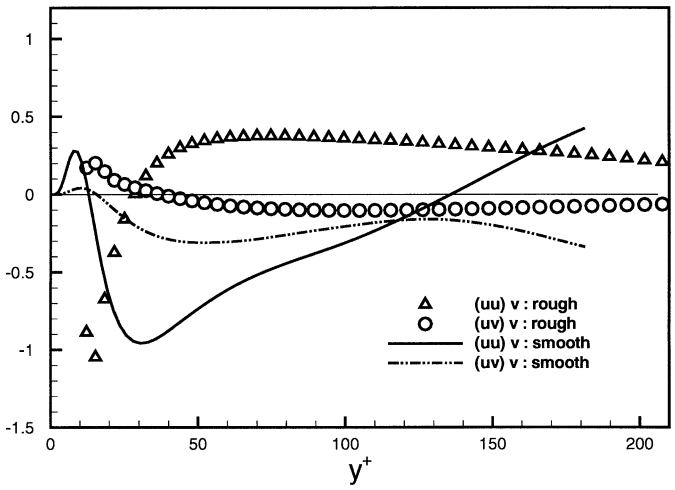

Figure 10. Reynolds stress transport terms, $\overline{u^2 v}$ and $\overline{u v^2}$ (transport terms in $\overline{u^2}$- and $\overline{uv}$-budget, respectively).

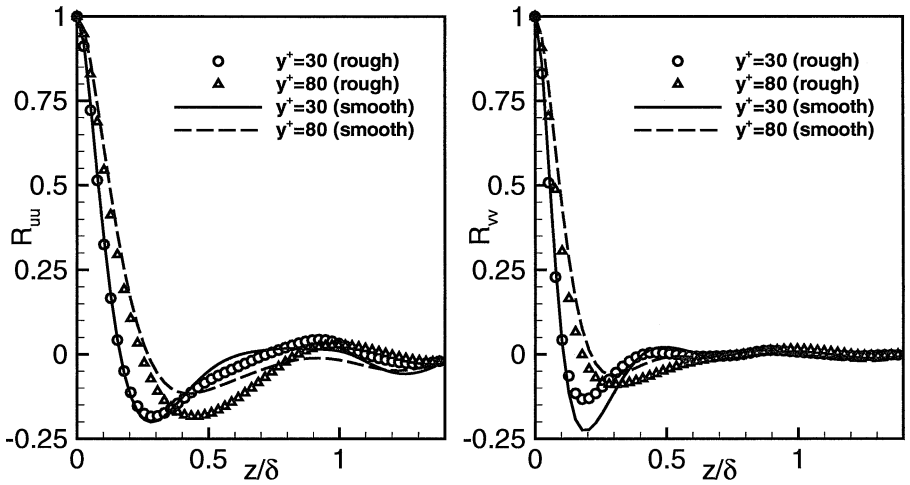

Figure 11. Two-point spanwise correlations with the separation distance normalized by the channel half-height.

wall-normal velocity components separated in the spanwise direction. The correlations are shown at wall-normal locations of $y^+ = 30$ and $y^+ = 80$. The separation distance is normalized by the channel half height. Normalized in this way, no discernible difference in the location corresponding to the negative peaks in R_{uu} and R_{vv} (respectively, corresponding to one half of the average streak spacing in the spanwise direction and the mean radius of the near-wall streamwise vortices) between the smooth- and rough-wall cases is seen, suggesting that the average streak spacing and the diameter of the streamwise vortices are not affected by the surface

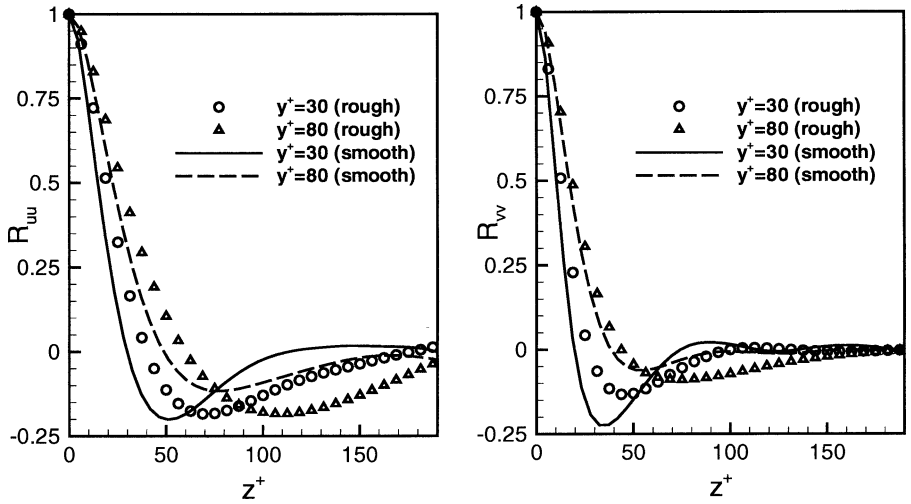

Figure 12. Two-point spanwise correlations with the separation distance normalized by local wall variables.

roughness. In Figure 12, on the other hand, the separation distance is normalized by the wall variables (local wall-shear velocity and kinematic viscosity). The two-point correlation for the streamwise velocity, R_{uu}, indicates that the streak spacing is increased to 140 wall units for the rough-wall case from the 100 wall units for the smooth-wall case at $y^+ = 30$. A similar trend of increased streak spacing is observed at $y^+ = 80$. Likewise, the two-point correlations of the wall-normal velocity, R_{vv}, indicates that the average diameter of the near-wall streamwise vortices is increased from 30 to 45 wall units at $y^+ = 30$, and a similar increase is observed at $y^+ = 80$. The streamwise extent of these structures can be estimated, similarly, from two-point correlations separated in the streamwise directions. Figure 13 shows R_{uu} and R_{vv} separated in the streamwise direction at $y^+ = 30$ and $y^+ = 80$. The separation distance is again normalized by the channel half-height. The length of the streaks decreases for the rough-wall case. Figure 14 shows the separation distance normalized by the wall variables. No significant difference is observed.

Figures 15 and 16 illustrate the comparison between streaks in the x-z plane for the rough-wall and the smooth-wall at two different y^+ locations, $y^+ = 5$ and 80. At $y^+ = 5$ the streaks are elongated on the smooth side of the channel, whereas at the same y^+ location the streaks look significantly different on the rough-wall side. At $y^+ = 80$, on the smooth-wall side of the channel the organized structures are not very apparent, whereas at the same y^+ location on the rough-wall side of the channel they appear more organized. This suggests that roughness results in organized structures for a larger y^+ compared to the no roughness case. Summarizing, the effects of roughness on streaks are as follows: in wall units, the streaks spacing increases in the spanwise direction, and the diameter of the

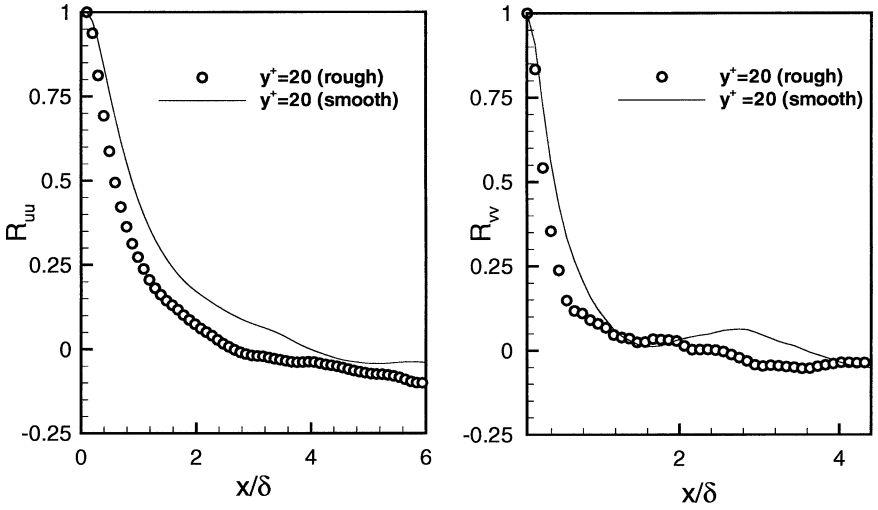

Figure 13. Two-point streamwise correlations with the separation distance normalized by channel half-height.

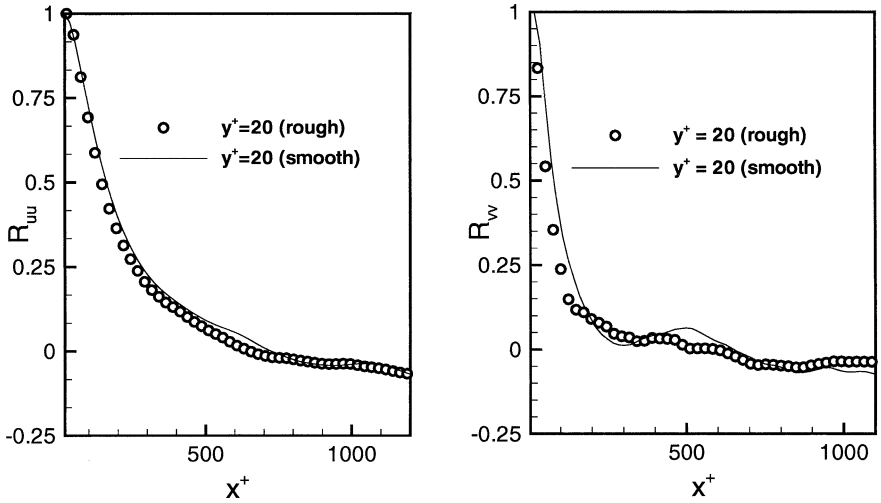

Figure 14. Two-point streamwise correlations with the separation distance normalized by local wall variables.

streamwise vortices (from R_{vv}) also increases. In physical units, the streaks extend to a larger y extent compared to the smooth-wall case.

Contour plots of u, v and w velocity components in an x-y plane were examined (not shown here) to investigate the effect of roughness on turbulence structures. The structure of the u component at the rough-wall side of the channel was distinctly different from the smooth-wall side in that increased activity were present near the rough-wall side. Contours of v indicated that the roughness resulted in more

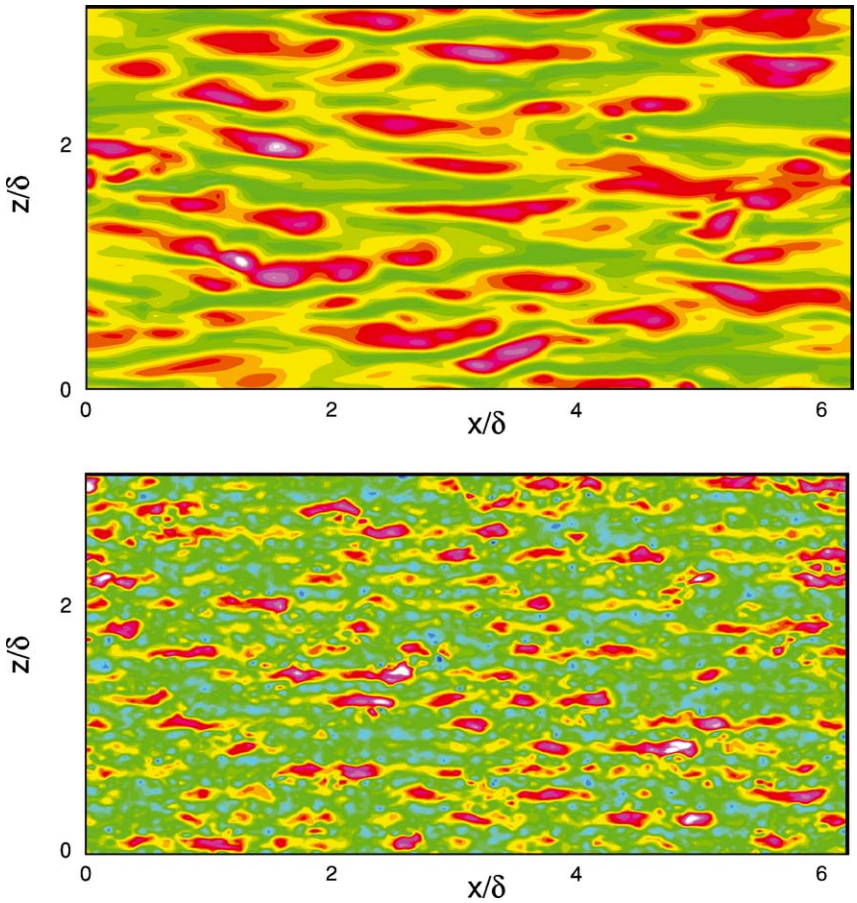

Figure 15. Contours of u at $y^+ = 5$ above the smooth-wall side (top) and the rough-wall side (bottom).

elongated structures along the wall-normal direction. This is consistent with the conclusions drawn from the statistical results, that roughness modifies the cross-shear transport process. The structure of the w component of velocity also indicated an increased activity on the rough-wall side of the channel, and a change in the angle of inclination of the structures. Figure 17 shows contour plots of the three vorticity components. The spanwise vorticity (ω_z) contours reveal that an irregular pattern of back flow is present both at the peak and valley locations of the roughness elements. The turbulence near the elements affects the vorticity on the bumps. The wall-normal vorticity (ω_y) contours show an organized pattern of dominant vorticity close to the peaks of the roughness bumps. From contours of velocity fluctuations (not shown) and Figure 17, it is apparent that the structures in the outer layer are significantly modified due to the presence of roughness. This further confirms the presence of communication between the inner and the outer layers of turbulence.

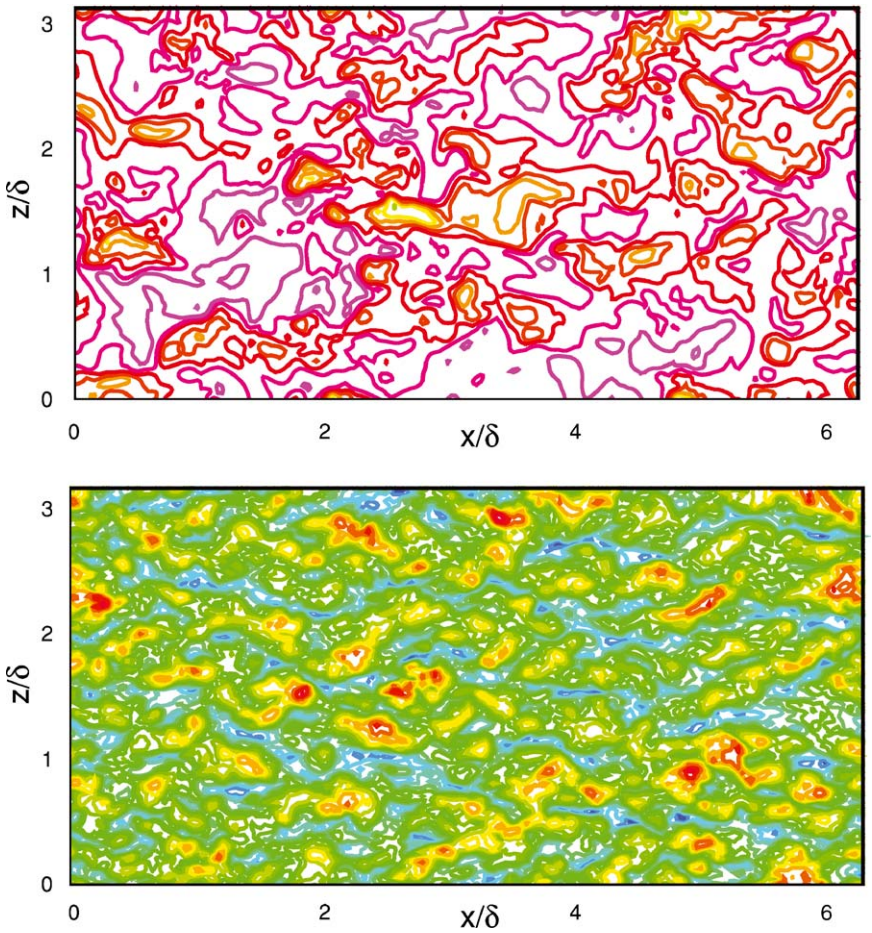

Figure 16. Contours of u at $y^+ = 80$ above the smooth-wall side (top) and the rough-wall side (bottom).

Contours of streamwise velocity and v-w velocity vectors in a y-z plane (not shown here) were also examined. The near-wall streamwise vortices were much stronger at the rough-wall side compared to those at the smooth-wall side. Increased turbulence activities at the rough-wall side were apparent. Different turbulence structures observed in the rough-wall region, especially the stronger streamwise vortices close to the roughness elements, led to the question of whether there is a fundamentally different self-sustaining mechanism by which turbulence is maintained in rough-wall-bounded turbulent flows. Our next step is to consider this possibility.

Kim and Lim [23] reported that the virtual flow without the linear coupling term between the wall-normal velocity and wall-normal vorticity contained no turbulence

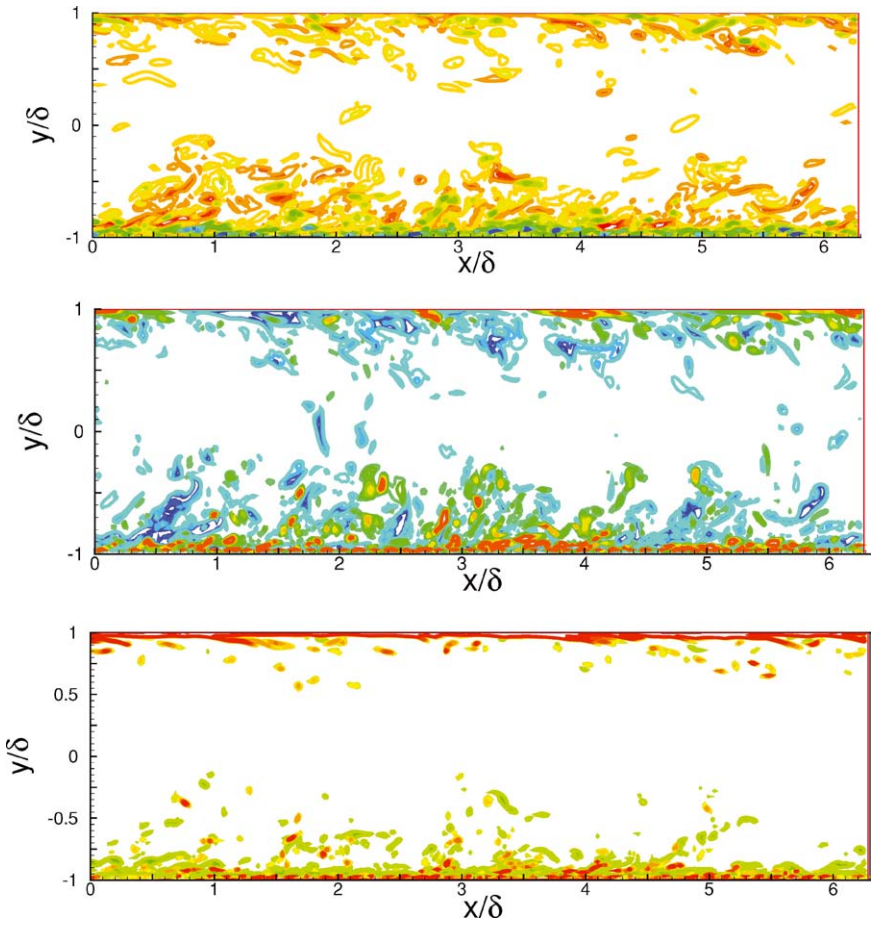

Figure 17. Contours of ω_x (top), ω_y (middle) and ω_z (bottom) in an x-y plane. The lower wall is the rough side of the channel and the upper wall is the smooth side of the channel.

structures (near-wall streamwise vortices and streaks in particular), resulting in complete laminarization of an initially turbulent channel flow. They concluded that the near-wall turbulence structures are maintained through the linear coupling term, without which turbulence cannot be sustained. We performed similar numerical experiments to investigate the role of the linear coupling term in the presence of surface roughness. We want to address the question of whether the linear coupling term continues to play an important role in maintaining near-wall turbulence in the presence of surface roughness.

A numerical experiment involved artificially removing the linear coupling term on the rough-wall side, while it was kept on the smooth-wall side. This numerical experiment was performed at $Re_\tau = 180$, since we wanted to compare the results with those in Kim and Lim [23]. Figure 18 shows the rms velocity fluctuations from this calculation. Substantial reductions are discernible in the rough-wall side,

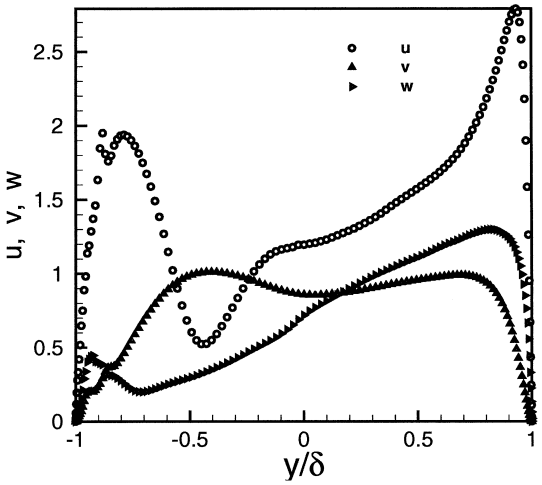

Figure 18. The rms velocity fluctuations with no linear coupling term on the rough-wall side (left half in the figure) of the channel.

where the coupling term is absent. However, the reduction—the streamwise component in particular—is much less compared to that observed in Kim and Lim's virtual flow. Apparently the surface roughness contributes directly to the maintenance of near-wall turbulence, thus preventing the complete laminarization found in the smooth-wall case. The rms vorticity fluctuations shown in Figure 19 indicate more substantial reductions in the vorticity fluctuations.

We also examine turbulence structures in the wall region to investigate the effects of surface roughness in the absence of the linear coupling term. Contour plots of

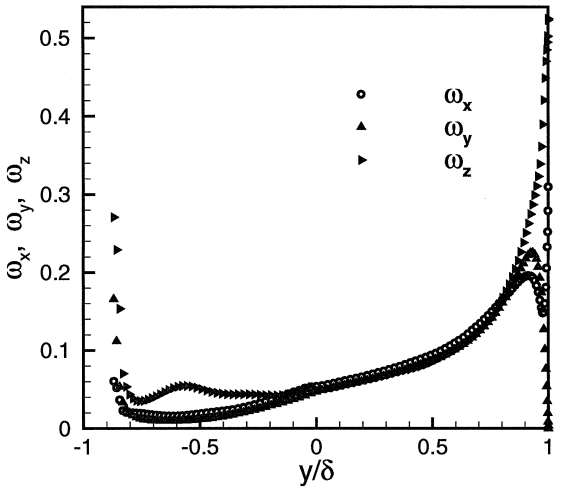

Figure 19. The rms vorticity fluctuations with no linear coupling term on the rough-wall side (left half in the figure) of the channel.

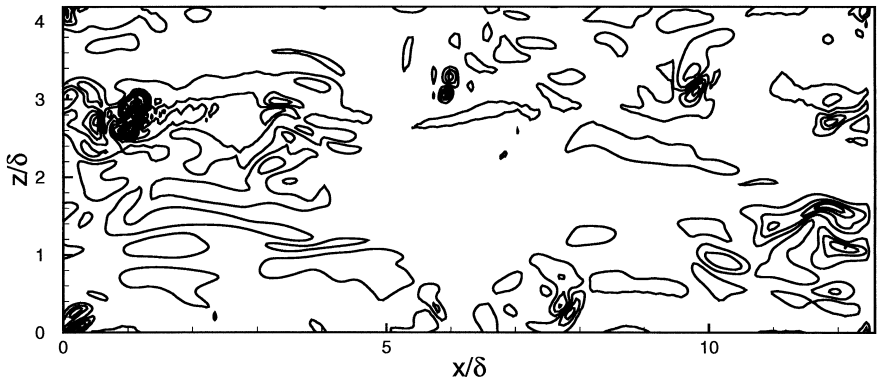

Figure 20. Contours of ω_y at $y^+ = 18$ above the rough-wall with no linear coupling term on the rough-wall side.

the wall-normal vorticity at $y^+ = 18$ on the rough-wall side of the channel (not shown here) revealed the usual high- and low-speed streaks. In contrast, the same contours from the rough wall without the linear coupling term showed no apparent turbulence structures, as shown in Figure 20. The same trends were observed from contour plots of other turbulence quantities in the x-z plane as well as those in x-y planes (not shown here), indicating that the usual dynamical activity of near-wall turbulence is absent without the linear coupling mechanism. It can be concluded from the observations—the suppression of the linear mechanism associated with the linear coupling term results in reduction of velocity and vorticity fluctuations and complete disappearance of the near-wall turbulence structures—that the self-sustaining mechanism of near-wall turbulence in the rough-wall channel is similar to that of the smooth-wall channel. The only additional effect of surface roughness is "kinematic effects" due to the presence of surface roughness. This has an important implication for turbulent boundary layer control: one can continue aiming at suppressing or reducing the linear mechanism due to the coupling term in designing a robust controller for drag reduction in rough-wall turbulent boundary layers, as was shown for the smooth-wall boundary layer by Kim [24].

3.3. ROUGHNESS SUBLAYER

The depth of the roughness sublayer is a subject of ongoing debate, and there is little information available on the characterization of the flow within this region. In this section we determine the depth of the sublayer for the large- and small-scale features of the flow. As the roughness elements in the x-z plane are represented by the double sine function, the averaging is performed at two different inhomogeneous locations—the "peak" and "valley" regions of corrugated surface. The underlying assumption is that the statistics at these two locations will yield a good estimate of the extent of inhomogeneity present in the layer. The rms velocity fluctuations are

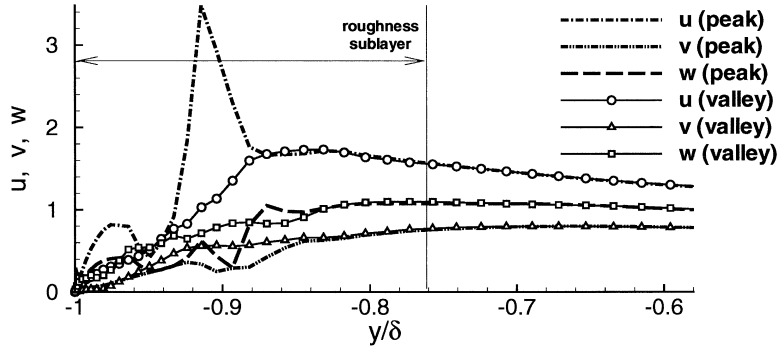

Figure 21. The rms velocity fluctuations normalized by u_τ at the smooth wall, shown above the peak and valley locations of roughness elements.

shown in Figure 21 at peak and valley locations of the corrugated surface. Spatial homogeneity is not achieved until $y/\delta = -0.82$. We performed this for three different roughness heights and obtained the depth of the roughness layer i.e $\zeta_{\text{large}}/\delta$ to be about $1.5h$, where subscript *large* represents the length scale for the large scale features of the flow, since it was revealed by a large-scale dominated statistics. A similar examination of the rms vorticity fluctuations revealed a somewhat smaller roughness sublayer, as shown in Figure 22. Spatial homogeneity of the small-scale structures is achieved at y/δ of -0.86, resulting in the depth of the roughness sublayer for small-scale roughness sublayer i.e $\zeta_{\text{small}}/\delta$ to be about $1.1h$; here the subscript *small* represents the length scale for the small scale features of the flow. It is worth noting that the horizontal components of the vorticity, ω_x and ω_z, exhibit significant spatial inhomogeneity due to the roughness elements, but that the wall-normal component of the vorticity ω_y does not.

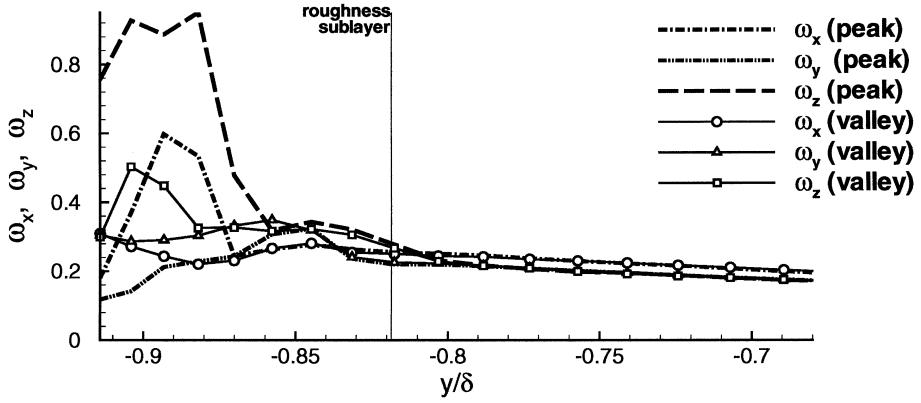

Figure 22. The rms vorticity fluctuations normalized by u_τ at the smooth wall, shown above the peak and valley locations of roughness elements.

Table I. Case study for varying l_z/δ with fixed $l_x/\delta = 0.6$ and $\rho = 0.21$.

Cases	l_z/δ
A1	0.5
A2	0.25
A3	0.12
A4	0.08
A5	0.02
A6	0.01

Table II. Case study for varying l_x/δ with fixed $l_z/\delta = 0.25$ and $\rho = 0.21$.

Cases	l_x/δ
B1	1.2
B2	0.8
B3	0.24
B4	0.04

4. Parametrization of the Roughness Surface

The roughness parameters that we will consider are the streamwise l_x and spanwise l_z size (i.e. wavelength) of the roughness elements (see Equation (4)) for a given roughness density (ρ), which is defined as the ratio of the area of the roughness elements in the horizontal plane at $y = \sigma_0$ to the total horizontal area. We chose the roughness elements to be ellipsoidal in shape, and so that we had the flexibility to vary the dimensions and the roughness density of these roughness elements. Considering that a large number of simulations had to be performed for this parametric study, all simulations were performed at $Re_\tau \approx 180$, based on u_τ at the smooth wall, using $192 \times 257 \times 192$ grid points in the streamwise ($L_x/\delta = 4\pi$), wall-normal, and spanwise ($L_z/\delta = 4\pi/3$) directions. Computed statistics for this Reynolds number revealed the same trend as those for $Re_\tau = 400$ presented in previous sections.

We began our study by varying the size of the elements in the spanwise direction, and with all the other parameters kept constant. We performed a case study for six different cases shown in Table I, where l_z/δ is varied from 0.5 to 0.01, with fixed $l_x/\delta = 0.6$ and $\rho = 0.21$. Figure 23 shows the mean velocity normalized by the local u_τ for all six cases plotted in wall units. For all the cases, the roughness function (ΔU^+) shows a negligible variation, indicating that that l_z/δ does not play a crucial role in determining the shift in the mean velocity profile. The roughness

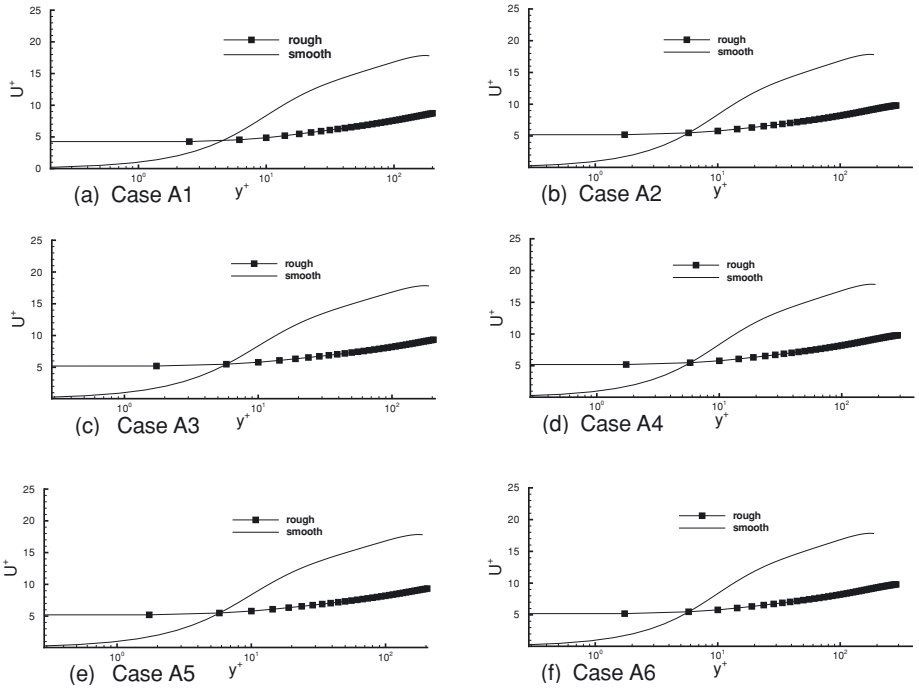

Figure 23. Mean velocity normalized by local u_τ for cases with varying l_z/δ and all other parameters fixed.

length scale y_0 (defined in Section 3), which is a surface property determined by roughness geometry, also indicates little variation with the size of the roughness elements in the spanwise direction. Figure 24 shows velocity fluctuations normalized by the local u_τ and δ_t. All six cases are shown. For Cases A1–A3, the u and w fluctuations are smaller on the rough-wall side compared to the smooth-wall side, while v fluctuations are larger on the rough-wall side close to the wall (i.e. inner layer). Away from the wall (outer layer), all three velocity components are smaller on the rough-wall side, which signifies that for these cases the outer layer of the turbulent boundary layer are also affected by the presence of roughness. For Cases A4–A6, all three velocity components in the inner layer show the same trend as the previous cases. In the outer layer, however, u and w fluctuations of the rough-wall side and smooth-wall side almost collapse, and the differences in the v fluctuations are not very large. The outer layer is not significantly affected by the presence of roughness for these cases. This leads to an interesting conclusion that the spanwise size of the roughness elements plays an important role in determining whether the outer layer is altered by roughness. The size of the roughness in the spanwise direction (normalized by the boundary layer thickness) does not play a significant role in mean velocity statistics, but it is significant to determine the nature of the velocity fluctuations, and hence the dynamics of the outer layers. This perhaps explains why

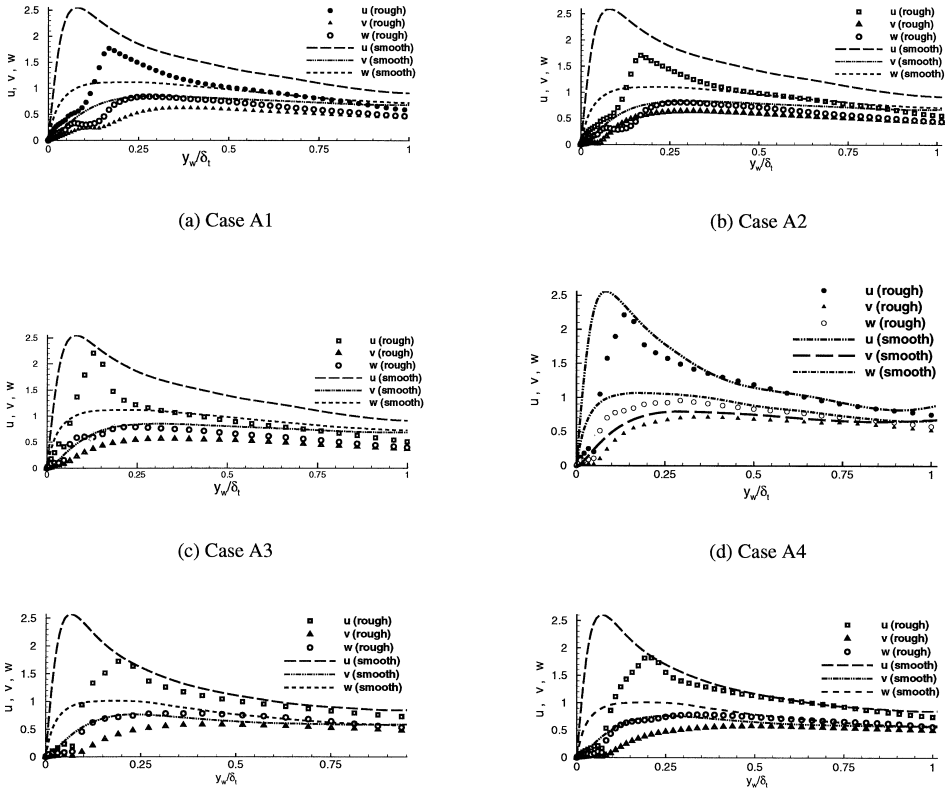

(a) Case A1

(b) Case A2

(c) Case A3

(d) Case A4

(e) Case A5

(f) Case A6

Figure 24. The rms velocity fluctuations normalized by local u_τ for cases with varying l_z/δ and all other parameters fixed.

many investigators with different roughness geometries obtained more or less similar roughness shifts of the mean velocity profile, but reported different results for the higher-orders statistics, such as the rms velocity fluctuations in the outer layer.

In the next set, we varied the size of the roughness elements in the streamwise direction but kept all the other parameters constant. (Table II). We fixed l_z/δ at two specific values, at $l_z/\delta = 0.25$ (where the outer layer statistics depended on the presence of roughness), and $l_z/\delta = 0.02$ (where the outer layer statistics did not). The mean velocity normalized by the local u_τ is shown in Figure 25. A slight variation in the roughness function (from 6.14 to 7.12) was observed. This is in contrast to the previous varying l_z case, but the trend is not very pronounced and more study is needed to determine the exact nature of the dependence of ΔU^+ with l_x. Figure 26 presents the rms velocity fluctuations. For all the cases, in the inner layer the u and w fluctuations for the rough-wall side are lower than the smooth-wall side, while the v fluctuations are higher. In the outer layer, all three velocity

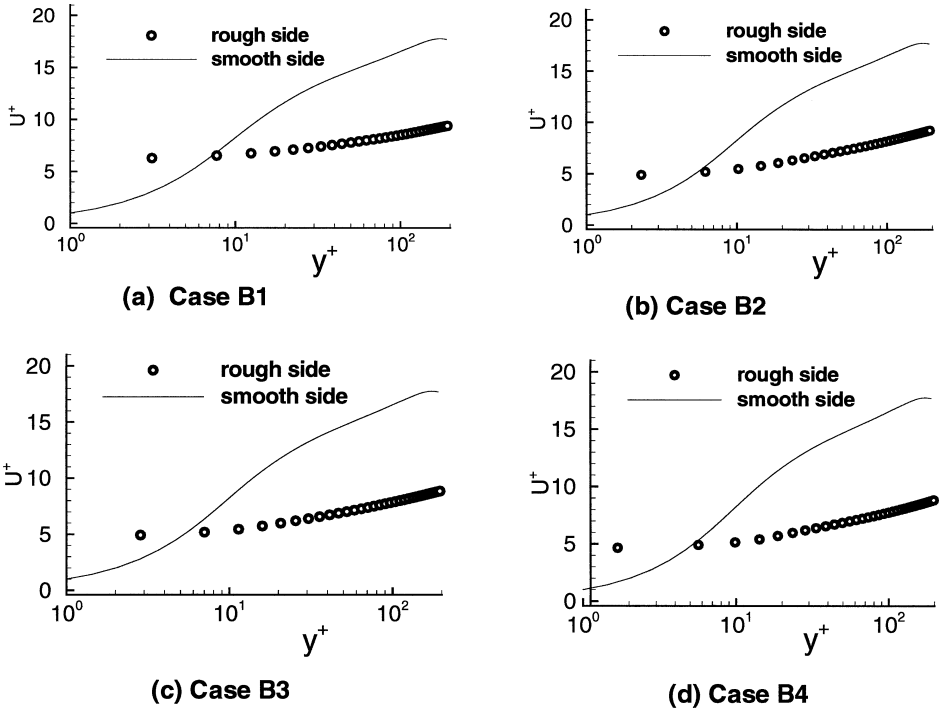

Figure 25. Mean velocity normalized by local u_τ for various l_x/δ with other parameters fixed.

components are lower for the rough-wall side compared to the smooth-wall side. The same test has been performed at a different $l_z/\delta = 0.02$. Results similar to Case A5 (Figure 24) have been observed, indicating that the physics in the outer layer is dominated by the size of the roughness element in the spanwise direction, rather than the size in the streamwise direction.

5. Summary and Concluding Remarks

Direct numerical simulations of a turbulent channel flow between a smooth and rough wall have been performed to investigate the effects of surface roughness on wall-bounded turbulence. To get a clearer picture of the impact of roughness in turbulent boundary layers, we have investigated the effects of 3D roughness arranged in an "egg carton" pattern. We performed a statistical analysis of the large- and small-scale features of the flow. When normalized by u_τ at the smooth-wall side, the rms velocity fluctuations at the rough-wall side are higher than the smooth-wall side. A similar effect is seen for the vorticity fluctuations. But when normalized by the local u_τ, the u and w fluctuations are smaller and the v fluctuation is higher for the rough-wall side in the inner layer, indicating a more isotropic state. In the outer layer all three velocity fluctuations are a smaller fraction of u_τ on the rough-wall side. The velocity fluctuations are thus altered throughout the boundary

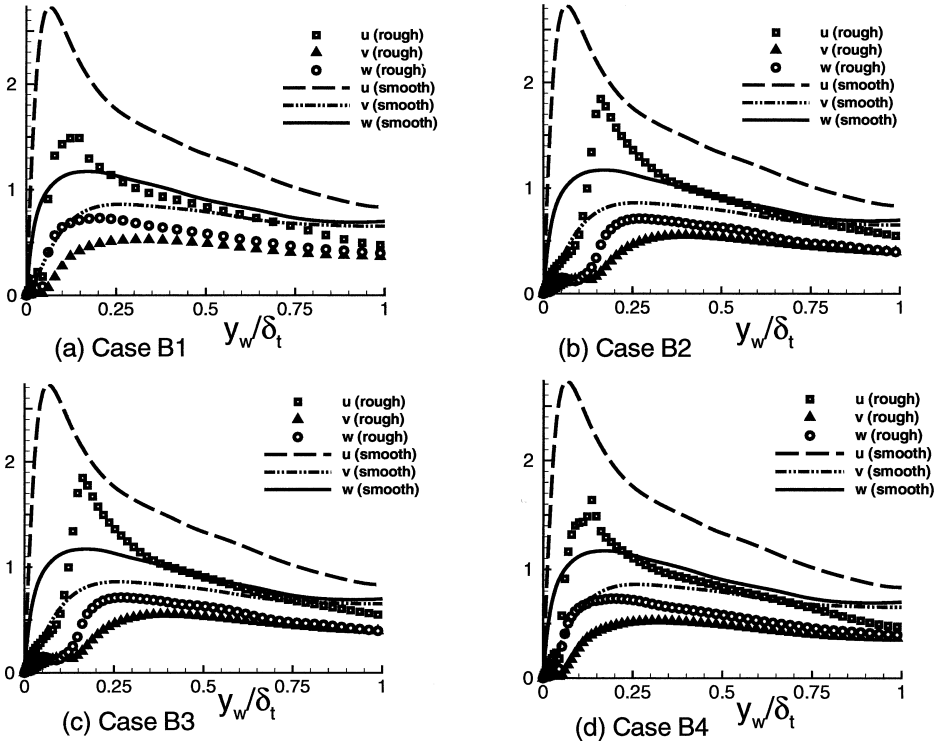

Figure 26. The rms velocity fluctuations normalized by local u_τ for various l_x/δ and all other parameters fixed.

layer due to the presence of roughness. The vorticity fluctuations, on the other hand, are not significantly altered in the outer layer, in that for both surfaces they exhibit the same dependence on u_τ and y_w/δ. Hence there is interaction between the inner and outer layers of the turbulent boundary layer at the large scales but not at the small scales. The results from the skewness and the transport terms of the Reynolds-stress budgets indicate modified wall-normal transport in the outer layer due to the roughness. Since the structures in the outer layer depend on whether the surface is smooth or rough, the present results can be added to the body of evidence that contradicts classical outer-layer similarity theory. The two-point correlations for the streamwise velocity reveal that the streak spacing in wall units increases for the rough-wall case. Likewise, the two-point correlations of the wall-normal velocity imply that the average diameter of the near-wall quasistreamwise vortices increases in terms of wall units. The correlation results also indicate that the mean streamwise length of the streaks decreases, measured with respect to local u_τ/ν, on the rough-wall side.

The thickness of the roughness sublayer depends on which statistic is used to characterize it. The roughness-induced inhomogeneity influences the velocity fluctuations (i.e. the larger scales) over a depth of 1.5 times the bump height h, while

the roughness sublayer defined by the small-scale-dominated vorticity fluctuations is $1.1h$.

One of the important conclusions that can be drawn from this study is that the streamwise and spanwise dimensions of roughness elements of fixed height play a crucial role in determining whether the roughness affects the outer layer. The spanwise size l_z/δ of the roughness does not influence the mean velocity statistics, but does have a large impact on the velocity fluctuations in the outer layer. This may explain why investigators with different roughness geometries can observe similar log-law shifts ΔU^+, but offer different interpretations of the outer-layer physics based on their observations of higher-order statistics in the outer layer.

Much of the present results summarized above are in agreement with previous experimental/numerical results or verify conjectures that have been proposed before. But some of the present results are at odds with some recent experimental results, which seem to indicate that the outer layer is unaffected by surface roughness. We have presented one plausible scenario how such difference can arise. There are other different factors (e.g. Reynolds number, different shapes and configurations of roughness elements) that can lead to different results. Much more work is needed for better understanding of the effect of roughness on wall-bounded turbulence.

Acknowledgments

This paper is a written version of the presentation by John Kim at an international conference on fluid mechanics, which was held in honor of Professor Robert Antonia on the occasion of his 60th birthday. John Kim acknowledges the fruitful collaborations he has had over the years with Professor Antonia. We are grateful to Professor Ian Castro for his comments on a draft of this manuscript, and to Dr. John Mansfied for his contribution to the immersed-boundary approach used in the present work. This work has been supported by Office of Naval Research (N00014-01-1-0811, Dr. Ronald Joslin). The computer time provided by NSF NPACI Centers (Blue Horizon at SDSC and Copper at NCSA) is also gratefully acknowledged.

References

1. Raupach, M.R., Antonia, R.A. and Rajagopalan, S., Rough-wall turbulent boundary layers. *Appl. Mech. Rev.* **44** (1) (1991) 1–20.
2. Wood, N. and Mason, P., The pressure force induced by neutral turbulent flow over hills. *Quart. J. Roy. Meteorol. Soc.* **119** (1993) 1233–1267.
3. Cheng, H. and Castro, I.P., Near wall flow over urban-like roughness. *Boundary-layer Meteorology* (2002) 229–257.
4. Perry, A.E., Lim, K.L. and Henbest, S.M., An experimental study of the turbulence structure in smooth- and rough-wall boundary layers. *J. Fluid Mech.* **177** (1987) 437–466.
5. Krogstad, P., Antonia, R.A. and Browne, W.B., Comparison between rough-and smooth-wall turbulent boundary layers. *J. Fluid Mech.* **245** (1992) 599–610.
6. Antonia, R.A. and Krogstad, P.A., Turbulence structure in boundary layers over different types of surface roughness. *Fluid Dyn. Res.* **28** (2001) 139–157.

7. Tachie, M.F., Bergstrom, D.J. and Balachandar, R., Rough wall turbulent boundary layers in shallow open channel flow. *J. Fluids Eng.* **122** (2000) 533–540.
8. Keirsbulck, L., Mazouz, A., Labraga, L. and Tournier, C., Influence of the surface roughness on the third-order moments of velocity fluctuations. *Exp. in Fluids* **30** (2001) 592–594.
9. George, J. and Simpson, R.L., Some effects of sparsely distributed three-dimensional roughness elements on two-dimensional turbulent boundary layers. AIAA Paper 2000–0915, (2000).
10. Ashrfian, A. and Andersson, H., DNS of turbulent flow in a rod-roughened channel. In: *Third International Symposium on Turbulence and Shear Flow Phenomena*, Sendai, Japan, June 25–27 (2003) Vol. 1, pp. 117–122.
11. Leonardi, S., Orlandi, P., Djenidi, L. and Antonia, R., Structure of turbulent channel flow with square bars on one wall, In: *Third International Symposium on Turbulence and Shear Flow Phenomena*, Sendai, Japan, June 25–27 (2003) pp. 123–128.
12. Shafi, H.S. and Antonia, R.A., Small-scale characteristics of a turbulent boundary layer over a rough wall. *J. Fluid Mech.* **342** (1997) 263–293.
13. Bandyopadhyay, R. and Watson, R.D., Structure of rough-wall turbulent boundary layers. *Phys. Fluids* **31** (1988) 1877–1880.
14. Mohd.-Yusof, J., Combined immersed-boundary/B-spline methods for simulations of flow in complex geometries. CTR-Annual Research Briefs, Stanford University/NASA, American Samoa (1997).
15. Fadlun, E.A., Verzicco, R., Orlandi, P. and Mohd-Yusof, J., Combined immersed-boundary/ finite-difference methods for three-dimensional complex flow simulations. *J. Comput. Phys.* **161** (2000) 35–60.
16. Goldstein, D., Handler, R. and Sirovich, L., Modeling a no-slip flow boundary with an external force field. *J. Comp. Phys.* **105** (1993) 354–366.
17. Verzicco. R. and Orlandi, P., A finite-difference scheme for three-dimensional incompressible flows in cylindrical coordinates. *J. Comp. Phys.* **123** (1996) pp. 402.
18. Kim, J., Moin, P. and Moser, R.D., Turbulence statistics in fully developed channel flow at low Reynolds number *J. Fluid Mech.* **177** (1987) 133–166.
19. Nikuradse, K., Stromungsgesetze in Rauhen Rohren. [English Trans. NACA Tech. Memo No. (1292).
20. Schlichting, H., *Boundary Layer Theory* 7th edn. (1979).
21. Krogstad, P. and Antonia, R.A., Surface roughness effects in turbulent boundary layers. *Expts. Fluids* **27** (2001) 450–460.
22. Keirsbulck, L., Labraga, L., Mazouz, A. and Tournier, C., Surface roughness effects on turbulent boundary layer structures., *J. Fluid Engrs.* **124** (2003) 127–135.
23. Kim, J. and Lim, J., A linear process in wall-bounded turbulent shear flows. *Phys. Fluids* **12**(8) (2000) 1885–1888.
24. Kim, J., Control of turbulent boundary layers. *Phys. Fluids* **15**(5) (2003) 1093–1105.
25. Krogstad, P. and Antonia, R.A., Structure of turbulent boundary layers on smooth and rough walls. *J. Fluid Mech*. **277** (1994) 1–20.